JACS
JOURNAL OF THE AMERICAN CHEMICAL SOCIETY
Article
pubs.acs.org/JACS

Factors That Control Catalytic Two- versus Four-Electron Reduction of Dioxygen by Copper Complexes

Shunichi Fukuzumi,*[,†,‡] Laleh Tahsini,[†] Yong-Min Lee,[†] Kei Ohkubo,[‡] Wonwoo Nam,*[,†] and Kenneth D. Karlin*[,†,§]

[†]Department of Bioinspired Science, Ewha Womans University, Seoul 120-750, Korea

[‡]Department of Material and Life Science, Graduate School of Engineering, Osaka University, ALCA, Japan Science and Technology Agency (JST), Suita, Osaka 565-0871, Japan

[§]Department of Chemistry, The Johns Hopkins University, Baltimore, Maryland 21218, United States

Supporting Information

ABSTRACT: The selective two-electron reduction of O_2 by one-electron reductants such as decamethylferrocene (Fc^*) and octamethylferrocene (Me_8Fc) is efficiently catalyzed by a binuclear Cu(II) complex $[Cu^{II}_2(LO)(OH)]^{2+}$ (**D1**) {LO is a binucleating ligand with copper-bridging phenolate moiety} in the presence of trifluoroacetic acid (HOTF) in acetone. The protonation of the hydroxide group of $[Cu^{II}_2(LO)(OH)]^{2+}$ with HOTF to produce $[Cu^{II}_2(LO)(OTF)]^{2+}$ (**D1-OTF**) makes it possible for this to be reduced by 2 equiv of Fc^* via a two-step electron-transfer sequence. Reactions of the fully reduced complex $[Cu^{I}_2(LO)]^{+}$ (**D3**) with O_2 in the presence of HOTF led to the low-temperature detection of the absorption spectra due to the peroxo complex $[Cu^{II}_2(LO)(OO)]$ (**D**) and the protonated hydroperoxo complex $[Cu^{II}_2(LO)(OOH)]^{2+}$ (**D4**). No further Fc^* reduction of **D4** occurs, and it is instead further protonated by HOTF to yield H_2O_2 accompanied by regeneration of $[Cu^{II}_2(LO)(OTF)]^{2+}$ (**D1-OTF**), thus completing the catalytic cycle for the two-electron reduction of O_2 by Fc^*. Kinetic studies on the formation of Fc^{*+} under catalytic conditions as well as for separate examination of the electron transfer from Fc^* to **D1-OTF** reveal there are two important reaction pathways operating. One is a rate-determining second reduction of **D1-OTF**, thus electron transfer from Fc^* to a mixed-valent intermediate $[Cu^{II}Cu^{I}(LO)]^{2+}$ (**D2**), which leads to $[Cu^{I}_2(LO)]^{+}$ that is coupled with O_2 binding to produce $[Cu^{II}_2(LO)(OO)]^{+}$ (**D**). The other involves direct reaction of O_2 with the mixed-valent compound **D2** followed by rapid Fc^* reduction of a putative superoxo-dicopper(II) species thus formed, producing **D**.

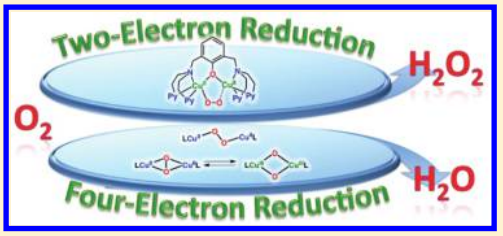

INTRODUCTION

Copper proteins that are involved in dioxygen (O_2) processing[1] possess highly evolved active-site environments, thus optimized via ligation with appropriate atom type (e.g., N, O, S), ligand charge (e.g., RS^- vs RSR′), the number of donors and their juxtaposition, resulting steric factors and second coordination shell influences,[2] all leading to the generation of specific $Cu_n(O_2)$ (n = typically 1−3) structures suitable for a particular function.[1f,3] The latter include O_2-transport ($Cu^{I}_2 + O_2 \rightleftarrows Cu_2(O_2)$) and substrate oxygenation (R−H → R−OH).[4] Another major class is copper oxidases, those effecting two-electron substrate oxidations (galactose oxidases[5] and amine oxidases)[6] while reducing O_2 to H_2O_2.[7] Meanwhile, multicopper oxidases (MCO's)[1a,1c,8] and heme-copper oxidases (HCO's)[9] facilitate $4e^-/4H^+$ reduction of dioxygen to water; the latter reactivity is analogously a fuel cell reaction.[10−16]

The ligand environment also defines the resulting chemistry for copper(I)−O_2 complexes, and dramatic tuning of O_2-adduct structure and reactivity may come via a change in chelate ligand denticity. Tetradentate nitrogen-based ligands typically provide for μ-1,2-peroxodicopper(II) adducts (**A**), tridentate chelates generally lead to side-on bound (μ-η^2:η^2)peroxo dicopper(II) complexes (**B**), and other tridentate or bidentate ligands support the formation of bis(μ-oxo)dicopper(III) Cu^{III}_2−$(O)_2$ complexes (**C**) (Scheme 1).[1f,3]

Scheme 1

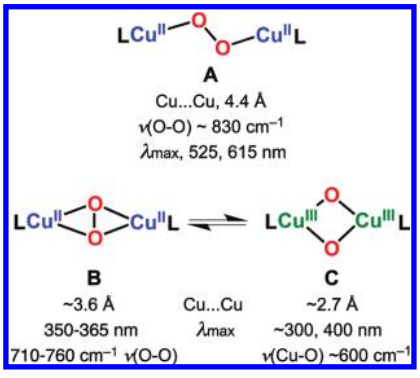

We recently became interested in examining discrete copper complexes as catalysts for $4e^-/4H^+$ O_2-reduction to water.[15,17] There is considerable interest in such catalysis, not only to aid the elucidation of fundamental principles relevant to biological

Received: December 14, 2011
Published: March 30, 2012

   dx.doi.org/10.1021/ja211656g | J. Am. Chem. Soc. 2012, 134, 7025−7035

processes (as above), but also due to the technological significance such as in fuel cell applications.[10−16,18] In fact, we found that ligand−(di)copper complexes forming **A**, **B**, or **C** (Scheme 1) can all catalyze the solution-phase $4e^-/4H^+$ O_2-reduction to water, employing ferrocenes reductants and acids as proton sources.[17] This methodology, as opposed to planting metal complexes onto electrode surfaces,[10−16,18] enables reaction mechanism elucidation via solution kinetic and spectroscopic monitoring of key steps occurring and intermediates forming during catalysis.[15,19−23]

Thus, $[\{(TMPA)Cu^{II}\}_2(\mu\text{-}1,2\text{-}O_2^{2-})]^{2+}$ (**A1**) (TMPA = tris(2-pyridylmethyl)amine) has structure **A** (Scheme 1), and, when formed, it is reductively O−O cleavaged (and protonated) to give water, in preference to simple protonation leading to H_2O_2.[17a,24] Precursor complexes leading to **B** or **C** are also catalysts for $4e^-/4H^+$ reduction of O_2.[17b] The course of reaction for $[Cu^{II}_2(N3)(H_2O)_2](ClO_4)_4$ [**B1**; N3 = $-(CH_2)_3$-linked bis[(2-(2-pyridyl)ethyl)amine]][25] versus $[Cu^{II}(BzPY1)(EtOH)](ClO_4)_2$ [**C1**; BzPY1 = *N*,*N*-bis[2-(2-pyridyl)ethyl]benzylamine][26] differs.[17b] One important finding is that for **B1**, the observed intermediate species, $[Cu^{II}_2(N3)(\mu\text{-}\eta^2\text{:}\eta^2\text{-}O_2^{2-})]^{2+}$, does not convert to the isomeric structure type **C**; rather, it is directly reduced by the ferrocenyl reductant leading to O−O cleavage to give water.

Thus far, there has been no report on the selective two-electron reduction of O_2 to H_2O_2 by one-electron reductants using copper complex catalysts. Herein, we describe such a case involving dicopper complex chemistry giving a fourth known Cu_2O_2 structural type.[1e,f,2] A reduced species $[Cu^{I}_2(LO)]^+$ (**D3**) reacts with O_2 to give $[Cu^{II}_2(LO)(OO)]^+$ (**D**),[28] which possesses an "end-on" peroxo-coordination (Scheme 2). The peroxo ligand in **D** is basic, and facile protonation leads to the μ-1,1-hydroperoxo dicopper(II) complex $[Cu^{II}_2(LO)(OOH)]^{2+}$ (**D4**) (Scheme 2).[29] As will be shown in this Article, this step is one of the keys to providing the observation of overall catalytic two-electron two-proton reduction of dioxygen to hydrogen peroxide (eq 1):

$$O_2 + 2e^- + 2H^+ \rightarrow H_2O_2(\text{catalytic}) \quad (1)$$

Scheme 2

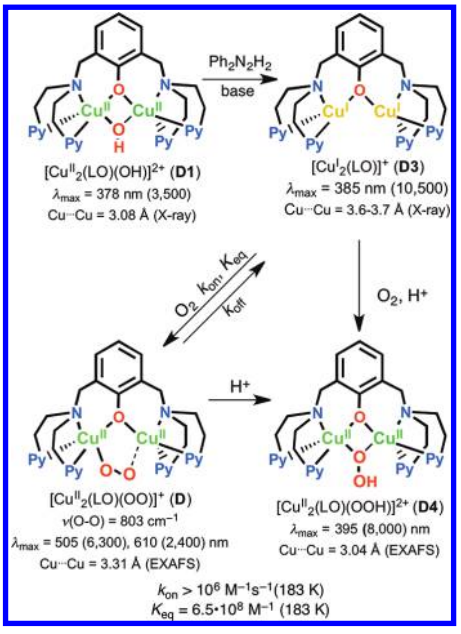

Further, we have been able to dissect this catalytic process, confirming the reaction stoichiometry, elucidating its kinetic behavior, and identifying various intermediates.

The insights obtained from this study and comparison to the $4e^-/4H^+$ O_2-reduction catalysis proceeding via O_2-complexes **A**, **B**, and **C** can or will allow us to explain how and why use of various ligands and their complexes leads to $4e^-/4H^+$ O_2-reduction, while others (or at least one other) provide for $2e^-/2H^+$ O_2-reduction to H_2O_2. The basics obtained here should serve as useful and broadly applicable principles for future design of catalysts for use in substrate oxidations and/or fuel cells, H_2O_2 itself as a product having considerable potential utility. Hydrogen peroxide has attracted increasing attention as a promising candidate as a sustainable and clean energy carrier,[30−33] because the free enthalpy change of the decomposition of hydrogen peroxide producing water and dioxygen is as large as −210.71 kJ mol^{-1}.[34] Hydrogen peroxide has also been used as a highly efficient and environmentally benign oxidant in terms of delignification efficiency and reducing ecological impact.[35,36]

EXPERIMENTAL SECTION

Materials. Grade quality solvents and chemicals were obtained commercially and used without further purification unless otherwise noted. Decamethylferrocene (Fc^*) (97%), octamethylferrocene (Me_8Fc), 1,1′-dimethylferrocene (Me_2Fc), ferrocene (Fc), hydrogen peroxide (50%), and HOTF (99%) were purchased from Aldrich Co., U.S., and NaI (99.5%) was from Junsei Chemical Co., Japan. Acetone was purchased from JT Baker, U.S., and used either without further purification for non-air-sensitive experiment or dried and distilled under argon and then deoxygenated by bubbling with argon for 30−45 min and kept over activated molecular sieve (4 Å) for air-sensitive experiments.[37] Preparation and handling of air-sensitive compounds were performed under Ar atmosphere (<1 ppm O_2, <1 ppm H_2O) in a glovebox (Korea Kiyon Co., Ltd.). The copper complexes $[Cu^{I}_2(LH)(CH_3CN)_2](SbF_6)_2$ (LH = *m*-xylene-linked bis[(2-(2-pyridyl)ethyl)amine])[27] as a precursor to $[Cu^{II}_2(LO)(OH)](SbF_6)_2$ (**D1**) and $[Cu^{I}_2(LO)]BArF$ (**D3**) ($BArF^-$ = $B(C_6F_5)_4^-$) for the low temperature generation of hydroperoxo species were prepared according to the literature procedures.[29] The use of $BArF^-$ rather than SbF_6^- as counteranion was due to the resulting higher stability and ease of handling of the air-sensitive dicopper(I) complex as well as the greater stability of the peroxo and hydroperoxo species that were then generated. Anal. Calcd for $(C_{36}H_{40}N_6O_2F_{12}Cu_2Sb_2)\cdot CH_3CN$: C, 37.15; H, 3.53; N, 7.98. Found: C, 37.24; H, 3.69; N, 8.32.

Instrumentation. UV−vis spectra were recorded on a Hewlett-Packard 8453 diode array spectrophotometer equipped with a UNISOKU Scientific Instruments Cryostat USP-203A for low-temperature experiments or an UNISOKU RSP-601 stopped-flow spectrometer equipped with a MOS-type highly sensitive photodiode array. Cyclic voltammetry (CV) and differential pulse voltammetry (DPV) measurements were performed on an ALS 630B electrochemical analyzer, and voltammograms were measured in deaerated acetone containing 0.20 M $TBAPF_6$ as a supporting electrolyte at −40 °C. The temperature was controlled by use of an MeCN/liquid N_2 bath. A conventional three-electrode cell was used with a gold working electrode (surface area of 0.3 mm^2), and a platinum wire was the counter electrode. The Au working electrode (BAS) was routinely polished with BAS polishing alumina suspension and rinsed with acetone before use. The potentials were measured with respect to the $Ag/AgNO_3$ (0.010 M) reference electrode. All potentials (vs Ag/Ag^+) were converted to values vs SCE by adding 0.29 V.[38] All electrochemical measurements were carried out under an atmospheric pressure of nitrogen. X-band EPR spectra were recorded at 5 K using an X-band Bruker EMX-plus spectrometer equipped with a dual mode cavity (ER 4116DM). Low temperature was achieved and controlled with an Oxford Instruments ESR900 liquid He quartz cryostat with an Oxford Instruments ITC503 temperature and gas flow controller. The experimental

dx.doi.org/10.1021/ja211656g | J. Am. Chem. Soc. 2012, 134, 7025−7035

parameters for EPR spectra were as follows: microwave frequency = 9.6483 GHz, microwave power = 1.0 mW, modulation amplitude = 10 G, gain = 5×10^2, modulation frequency = 100 kHz, time constant = 81.92 ms, and conversion time = 81.00 ms.

Kinetic Measurements. The spectral change in the UV−visible was recorded on a Hewlett-Packard 8453 diode array spectrophotometer equipped with Unisoku thermostatted cell holder for low-temperature experiments. In a typical catalytic reaction, the quartz cuvette is loaded with 3 mL of 10:30:1 Fc^*/HOTF/**D1** (1.0×10^{-4} M) in a degassed solution of acetone. O_2 gas (99.999%) was then introduced into the solution through a needle for 1 min to make it O_2-saturated. The catalytic reaction is monitored by the increase in the absorbance at 780 nm corresponding to the formation of the ferrocenium cation (Fc^{*+}) ($\varepsilon = 5.8 \times 10^2$ M^{-1} cm^{-1}). The ε value of Fc^{*+} was confirmed by the electron-transfer oxidation of Fc^* with *p*-benzoquinone in the presence of HOTF (see Figure S1 in the Supporting Information).

The limiting concentration of O_2 in an acetone solution was prepared by injecting a different aliquot of an O_2-saturated acetone solution (1.1×10^{-2} M),[39] prepared by bubbling O_2 through argon-saturated acetone in a Schlenk tube for 30 min at 298 K.[40] In case of the experiment involving 2.2 equiv of O_2 relative to **D1** (1.0×10^{-4} M), 60 μL of the O_2-saturated acetone solution was injected into the cuvette with the total volume of 3 mL.

Iodometric Titration for the Determination of H_2O_2. The amount of H_2O_2 was determined by titration with iodide ion.[41] The diluted acetone solution (1/15) of the reduced product of O_2 was treated with an excess of NaI. The amount of I_3^- formed was then quantified using its visible spectrum (λ_{max} = 361 nm, $\varepsilon = 2.5 \times 10^4$ M^{-1} cm^{-1}). The controlled reactions including the reaction of **D1** complex with NaI, H_2O_2 with NaI in the absence of **D1**, and H_2O_2 with NaI in the presence of **D1** were also performed to elucidate the exact amount of H_2O_2 generated in the catalytic two-electron reduction of O_2 by Fc^*.

Low-Temperature Experiments Concerning the Generation of $[Cu^{II}_2(LO)(OOH)]^{2+}$ (D4). Under an argon atmosphere within a glovebox, $[Cu^{I}_2(LO)]BArF$ (**D3**) (7.0×10^{-5} M) was dissolved in 3 mL of O_2-free acetone giving a bright yellow solution. The cuvette was fully sealed with a septum and quickly removed from the glovebox and cooled to −80 °C in a Hewlett-Packard 8453 diode array spectrophotometer equipped with Unisoku thermostatted cell holder. O_2 was gently bubbled through the reaction solution, and 1 equiv of HOTF dissolved in CH_2Cl_2 was quickly added by syringe. The formation of the hydroperoxo species was followed by the change in the absorbance at 395 nm. The ε value of $[Cu^{II}_2(LO)(OOH)]^{2+}$ (**D4**) was determined to be 1.0×10^4 M^{-1} cm^{-1} measured in acetone at −80 °C.

Low-Temperature Experiments Concerning the Reaction of Mixed-Valence $[Cu^{II}Cu^{I}(LO)]^{2+}$ (D2) with O_2. Under an argon atmosphere within a glovebox, **D1** (1.0×10^{-4} M) was mixed with Fc^* (1.0×10^{-4} M) and TFA (1.0×10^{-3} M) in 3 mL of O_2-free acetone, giving an orange solution. The cuvette was fully sealed with septum and quickly removed from the glovebox and cooled to −80 °C. O_2 gas was then gently bubbled through the solution using a needle. The formation of the hydroperoxo species was followed by the change in the absorbance at 395 nm.

DFT Calculations. Density-functional theory (DFT) calculations were performed on a 32CPU workstation (PQS, Quantum Cube). Geometry optimizations were carried out using the Becke3LYP functional and lanl2dz basis set as implemented in the Gaussian 09 program revision A.02.[42] Graphical outputs of the computational results were generated with the Gauss View software program (ver. 3.09) developed by Semichem, Inc.[43]

RESULTS AND DISCUSSION

Mechanism of D1-Catalyzed Two-Electron Reduction of O_2 with Fc^* to H_2O_2. For the sake of clarifying and a better understanding of this study, we prefer to present the mechanism of $[Cu^{II}_2(LO)(OH)]^{2+}$ (**D1**)-catalyzed two-electron reduction of O_2 with Fc^* at the beginning, as shown in Scheme 3. What follows is our presentation of how the observations and data lead to this catalytic mechanism.

Scheme 3. Reaction Sequence Deduced for the Catalytic Two-Electron Two-Proton Reduction of O_2 to H_2O_2[a]

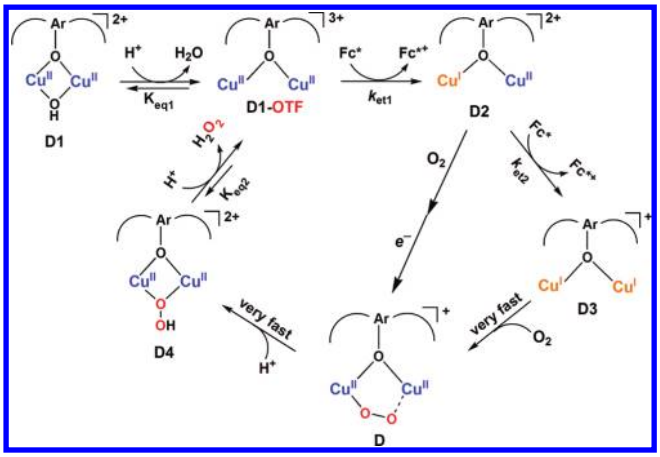

[a]The initial catalyst is $[Cu^{II}_2(LO)(OH)](SbF_6)_2$ (**D1**), and the reaction is carried out in acetone solution using decamethylferrocene (Fc^*) as reductant and trifluoroacetic acid (HOTF) as proton source. See text for further details, including the "short-circuit" path from **D2** to **D**.

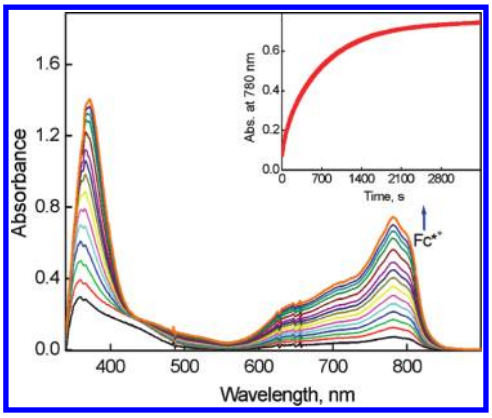

Figure 1. UV−vis spectral changes observed in the two-electron reduction of O_2 catalyzed by $[Cu^{II}_2(LO)(OH)]$ (**D1**) (0.040 mM) with Fc^* (1.0 mM) in the presence of HOTF (3.0 mM) in O_2-saturated acetone ($[O_2]$ = 11.0 mM) at 223 K. The inset shows the time profile of the absorbance at 780 nm due to Fc^{*+}.

No oxidation of Fc^* by O_2 occurred in the absence and presence of $[Cu^{II}_2(LO)(OH)]^{2+}$ (**D1**) in acetone (Figure S2 in the Supporting Information). However, when trifluoroacetic acid (HOTF) was added to the Fc^*−O_2−**D1** system at 223 K, efficient oxidation of Fc^* by O_2 occurred to yield Fc^{*+} as indicated by an increase in the absorbance at 780 nm due to Fc^{*+} (Figure 1). When more than 2 equiv of Fc^* relative to O_2 (i.e., limiting $[O_2]$) were employed,[39] still only 2 equiv of Fc^{*+} (λ_{max} = 780 nm) formed, even in the presence of excess HOTF (Figure S3 in the Supporting Information). The stoichiometry of the catalytic oxidation of Fc^* by O_2 is given by eq 1 (Introduction). The formation of H_2O_2 was confirmed by iodometric titration (Figure S4 in the Supporting Information). The amount of I_3^- produced (λ_{max} = 360 nm) was the same as that produced by the reaction of the stoichiometric amount of H_2O_2 with I^- (Figure S5 in the Supporting Information).

dx.doi.org/10.1021/ja211656g | J. Am. Chem. Soc. 2012, 134, 7025−7035

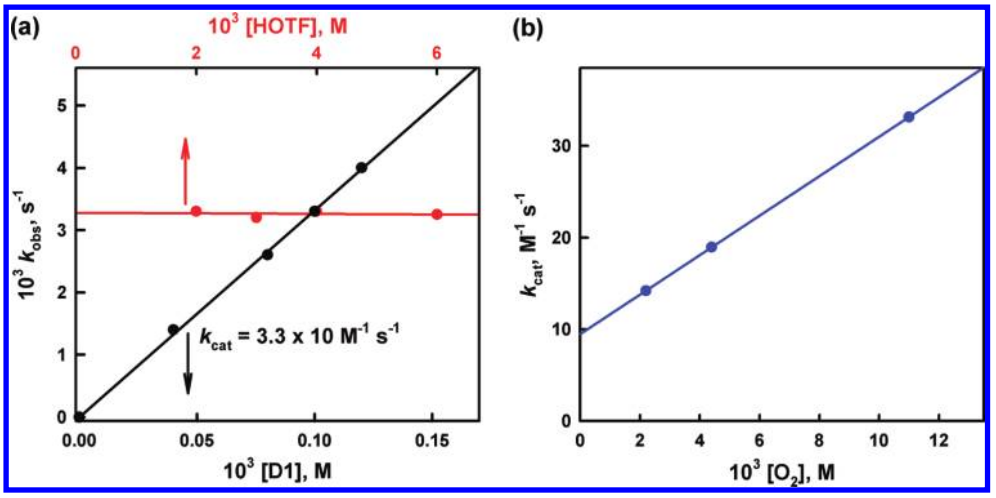

Figure 2. (a) Plot of the pseudo-first-order rate constants (k_{obs}) versus concentrations of **D1** (black line) to determine second-order rate constant (k_{cat}) for the two-electron reduction of O_2 catalyzed by **D1** with Fc^* (1.0 mM) in the presence of TFA (3.0 mM) in O_2-saturated acetone ($[O_2]$ = 11.0 mM) at 223 K. The red line shows the plot of k_{obs} versus concentrations of TFA in the two-electron reduction of O_2 catalyzed by **D1** (0.10 mM) with Fc^* (1.0 mM) in the presence of TFA in O_2-saturated acetone ($[O_2]$ = 11.0 mM) at 223 K. (b) Plot of k_{cat} versus concentrations of O_2 in the two-electron reduction of O_2 catalyzed by **D1** (0.10 mM) with Fc^* (1.0 mM) in the presence of TFA (3.0 mM) in acetone at 223 K.

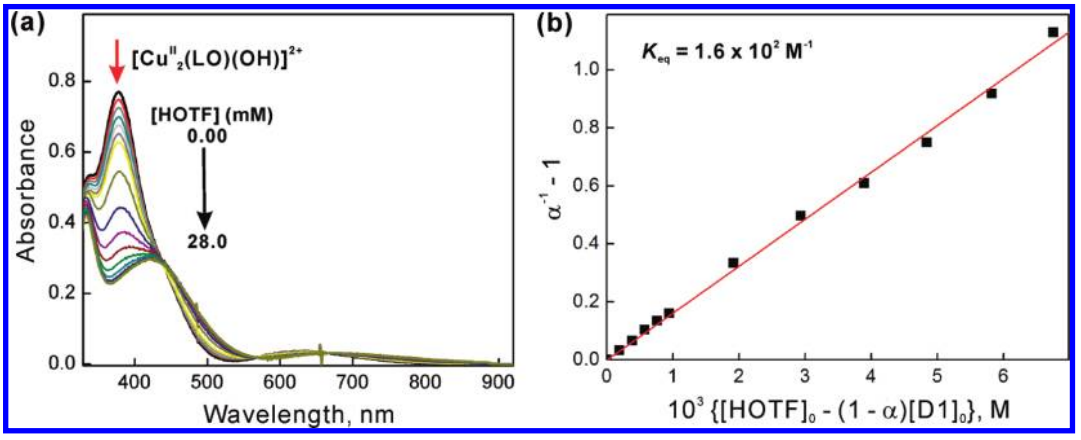

Figure 3. (a) UV−visible spectral changes of $[Cu^{II}_2(LO)(OH)]$ (**D1**) (0.20 mM) in the presence of HOTF (0.0−28.0 mM) in acetone at 298 K. (b) Plot of $\alpha^{-1} - 1$ versus $\{[HOTF]_0 - (1 - \alpha)[\mathbf{D1}]_0\}$ to determine the equilibrium constants (K_{eq}) in the protonation of **D1** upon addition of TFA (0.0−28.0 mM) into the solution of **D1** (0.20 mM) in acetone at 298 K.

Thus, selective two-electron reduction of O_2 with Fc^* occurred in the presence of excess HOTF and a catalytic amount of **D1** in acetone at 223 K. When the temperature was raised to 298 K, the yield of H_2O_2 decreased to 55% because of competition with the direct reduction of H_2O_2 by Fc^* (Figure S6 in the Supporting Information). Thus, the kinetic analyses were performed at 223 K (vide infra).

The rate of formation of Fc^{*+} (inset of Figure 1) obeyed first-order kinetics (Figure S7 in the Supporting Information). The observed first-order rate constant increased linearly with increasing concentration of the catalyst (**D1**) as shown in Figure 2a. The dependence of k_{obs} on concentration of HOTF was also examined, and the results are shown in Figure 2a, where the k_{obs} value remains the same with increasing concentration of HOTF. The dependence of k_{obs} on concentration of O_2 is shown in Figure 2b, where the k_{obs} value increases linearly with increasing concentration of O_2 and a clear intercept is recognized (Figure S8 in the Supporting Information). Thus, the rate of formation of Fc^{*+} is given by eq 2:

$$d[Fc^{*+}]/dt = k_{cat}[\mathbf{D1}][Fc^*] \quad (2)$$

$$k_{cat} = k_1 + k_2[O_2] \quad (3)$$

where k_{cat} is the second-order catalytic rate constant, k_1 corresponds to the second-order rate constant, which is independent of concentration of O_2, and k_2 corresponds to the rate constant, which is dependent on concentration of O_2. In the next section, each step in the catalytic cycle in Scheme 3 is examined in detail to reconcile the kinetic formulation given by eqs 2 and 3.

Protonation of $[Cu^{II}_2(LO)(OH)](SbF_6)_2$ (D1). Because no oxidation of Fc^* by O_2 occurred in the presence of **D1** without added acid, a spectral titration of **D1** with HOTF was carried out (Figure 3a). The result is that the absorption band at 378 nm due to $[Cu^{II}_2(LO)(OH)]^{2+}$ is red-shifted to 420 nm; a clean isosbestic point is observed at 430 nm. This spectral change is well analyzed by assuming formation of the protonated complex $[Cu^{II}_2(LO)(OTF)]^{2+}$ (**D1-OTF**); confirming evidence comes from a separate examination of the 1:1 reaction of HOTF with authentic **D1**.[44] The protonation constant (K) of **D1** to produce **D1-OTF** is determined by eq 4, where $[\mathbf{D1}]_0 = [\mathbf{D1}] + [\mathbf{D1}\text{-HOTF}]$, and $[\mathbf{D1}]_0$ and $[HOTF]_0$ are the initial concentrations of **D1** and HOTF. Equation 4 is easily converted to eq 5, where $\alpha = [\mathbf{D1}]/[\mathbf{D1}]_0 = \Delta A/\Delta A_0$ (ΔA is the absorbance change at

dx.doi.org/10.1021/ja211656g | J. Am. Chem. Soc. 2012, 134, 7025−7035

378 nm due to **D1**, and ΔA_0 corresponds to the absorbance change when all **D1** molecules are converted to **D1-OTF**). A linear correlation between $\alpha^{-1} - 1$ versus $[\mathrm{HOTF}]_0 - (1 - \alpha)[\mathbf{D1}]_0$ shown in Figure 3b confirmed the validity of the assumption of the formation of $Cu^{II}_2(LO)(OTF))^{2+}$ (**D1-OTF**). Next, the K value is determined from the slope of a linear plot of $\alpha^{-1} - 1$ versus $[\mathrm{HOTF}]_0 - (1 - \alpha)[\mathbf{D1}]_0$ (Figure 3b) to be 1.6×10^2 M^{-1}. The temperature dependence of K was examined (Figure S9 in the Supporting Information), and the van't Hoff plot (Figure S10 in the Supporting Information) afforded $\Delta H = -3.6$ kcal mol^{-1} and $\Delta S = 2.1$ cal K^{-1} mol^{-1}.

$$K = [\mathbf{D1}{-}\mathrm{HOTF}]/[\mathbf{D1}][\mathrm{HOTF}] = ([\mathbf{D1}]_0 - [\mathbf{D1}])/\{([\mathrm{HOTF}]_0 - [\mathbf{D1}]_0 + [\mathbf{D1}])[\mathbf{D1}]\} \quad (4)$$

$$\alpha^{-1} - 1 = K\{[\mathrm{HOTF}]_0 - (1 - \alpha)[\mathbf{D1}]_0\} \quad (5)$$

The binuclear Cu(II) complex $[Cu^{II}_2(LO)(OH)]$ (**D1**) is EPR silent because of antiferromagnetic coupling of the two Cu(II) ions. The protonated complex **D1-OTF** was also EPR silent (Figure S11 in the Suppporting Information). This indicates that two Cu(II) ions still maintain an electronic/magnetic interaction after the protonation of **D1**. Because the catalytic reduction of O_2 by Fc^* with **D1** was made possible only by the presence of TFA, the effect of protonation of **D1** by TFA on the one-electron reduction of **D1** was examined by cyclic voltammetry (CV) and difference pulse voltammetry (DPV) measurements. Figure 4a shows a CV of **D1** in acetone at 233 K. The irreversible cathodic peak current was observed at −0.71 V vs SCE at a sweep rate of 0.10 V s^{-1}, while the DPV exhibits the cathodic peak at −0.68 V vs SCE. The cathodic peak is much more negative as compared to the one-electron oxidation potential of Fc^* (E_{ox} = −0.08 V vs SCE).[45−47] This is the reason why no electron transfer from Fc^* to **D1** ensues, thus precluding copper(I) formation, O_2-reaction, and Fc^* oxidation.

In the presence of HOTF, however, the DPV peak is shifted to a positive direction as shown in Figure 4b, where a first and also a second one-electron reduction peak for $[Cu^{II}_2(LO)(OTF)]^{2+}$ (**D1-OTF**) are observed at 0.18 and 0.00 V vs SCE, respectively. This implied that a mixed-valence complex $[Cu^{II}Cu^{I}(LO)]^{2+}$ (**D2**) may (and does) form (vide infra). In the presence of O_2, a catalytic current for the reduction of O_2 is observed at −0.02 V, which corresponds to the second one-electron reduction of **D1-OTF** (Scheme 3), and the catalytic current increases with increasing concentration of O_2 (Figure 4b).

Two-Step Electron Transfer from Fc^* to $Cu^{II}_2(LO)(OTf)]^{2+}$ (D1-OTF). As was said, the E_{ox} value of Fc^* is more negative than the first and second one-electron potentials of **D1-OTF**, making electron transfer from Fc^* to **D1-OTF** thermodynamically feasible. Thus, we examined the dynamics of electron transfer from Fc^* to **D1-OTF**. In fact, electron transfer from Fc^* to **D1** in the presence of HOTF occurs by a two-step process, this not being unexpected based on the observation that two one-electron reduction peaks are observed, Figure 4b. Figure 5 shows the UV−vis changes corresponding to the first step in the presence of 2.0 mM HOTF at 203 K. At this temperature, most **D1** molecules are converted to **D1-OTF** with 2.0 mM HOTF. The amount of Fc^{*+} produced in the first electron transfer from Fc^* to **D1-OTF** is the same as the concentration of **D1** (0.10 mM). The rate of formation of Fc^{*+} obeyed pseudo-first-order kinetics at the initial stage of the reaction in the presence of HOTF (3.0 mM) in

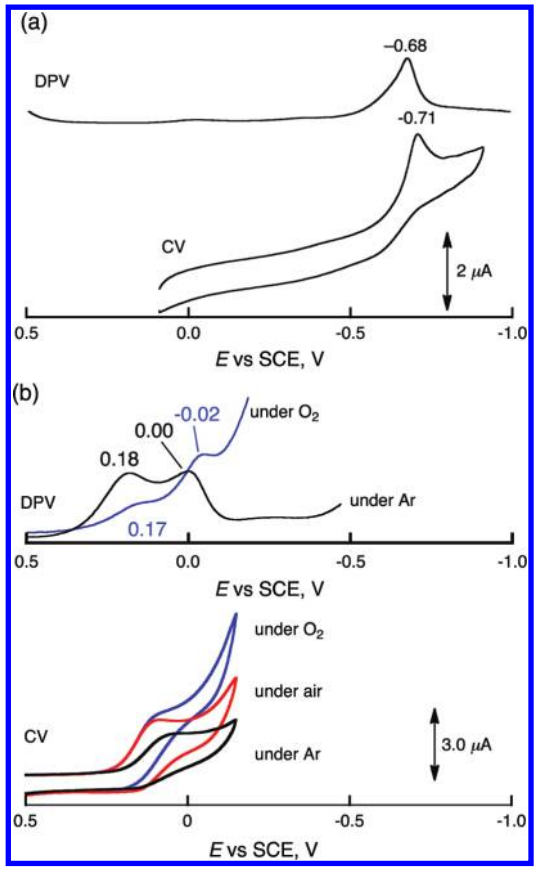

Figure 4. (a) Cyclic voltammograms and differential pulse voltammograms (DPV) of **D1** (2.0 mM) in the absence of HOTF in deaerated acetone at 233 K. (b) CV and DPV of **D1** (2.0 mM) in the presence of HOTF (50 mM) in deaerated (black), air-saturated (red), and O_2-saturated (blue) acetone at 233 K. $TBAPF_6$ (0.20 M) was used as an electrolyte.

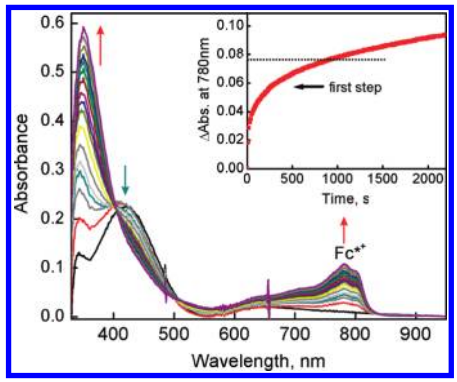

Figure 5. UV−vis spectral changes observed in the electron transfer from Fc^* (0.40 mM) to $[Cu^{II}_2(LO)(OH)]$ (**D1**) (0.10 mM) in the presence of HOTF (2.0 mM) at 203 K. The inset shows the time profile of the absorbance at 780 nm due to Fc^{*+}, showing that 1 equiv of Fc^{*+} is formed in the first step, that is, first phase. Note: The nonzero absorbance at 780 nm before the mixing of **D1** and Fc^* is due to the d−d transition of **D1** complex, causing a large increase when the initial spectrum was recorded. This absorbance was subtracted from the total absorbance to give the absorbance due to Fc^{*+} to determine the rate constant.

acetone at 203 K (Figure S12 in the Supporting Information). The observed pseudo-first-order rate constant (k_{obs}) increases linearly with increasing the concentration of Fc^* (Figure 6). The second-order rate constant (k_{et1}) of electron transfer from Fc^* to **D1-OTF** was determined to be 7.8 M^{-1} s^{-1} from the slope of a linear plot of k_{obs} versus $[Fc^*]$ at 203 K.

dx.doi.org/10.1021/ja211656g | J. Am. Chem. Soc. 2012, 134, 7025−7035

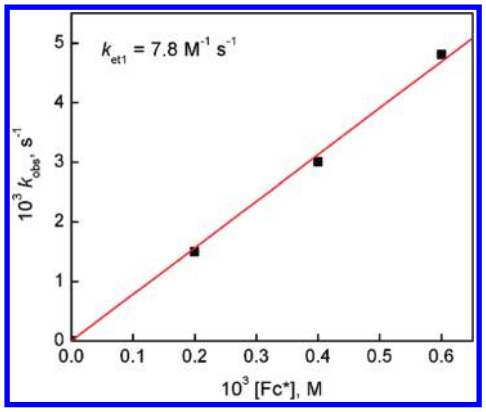

Figure 6. Plot of the pseudo-first-order rate constants (k_{obs}) versus concentrations of Fc^* in the first electron transfer from Fc^* to $[Cu^{II}_2(LO)(OH)]$ (**D1**) (0.10 mM) to determine the k_{et1} value in the presence of HOTF (2.0 mM) in acetone at 203 K.

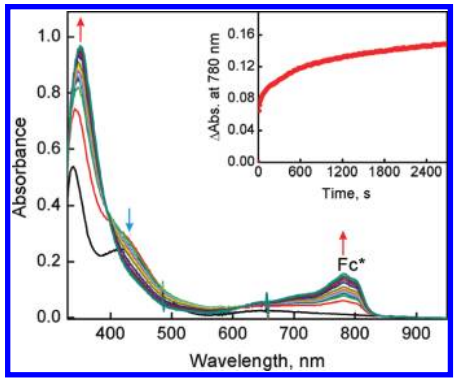

Figure 7. UV−vis spectral changes observed in the electron transfer from Fc^* (1.2 mM) to $[Cu^{II}Cu^{I}(LO)]^{2+}$ (**D2**) (0.10 mM), formed as described in the text, in the presence of HOTF (2.0 mM) at 213 K. The inset shows the time profile of the absorbance at 780 nm due to Fc^{*+}. Note: The nonzero absorbance at 780 nm before the mixing of **D2** and Fc^* is due to a d−d transition of this complex, and this causes a large increase in recording of the first spectrum. For practical reasons, this absorbance is subtracted from the total absorbance to give the absorbance due to Fc^{*+} to calculate the rate constant.

Figure 7 shows UV−vis monitoring of the second step of electron transfer from Fc^* to **D1-OTF**, which corresponds to electron transfer from Fc^* to the mixed-valence complex, $[Cu^{II}Cu^{I}(LO)]^{2+}$ (**D2**). This could be separately generated by the one-electron reduction of **D1** with 1 equiv of Fc^* in the presence of excess HOTF. EPR spectroscopic measurements confirmed the generation of **D2**, as this new species only exhibits signals due to the one Cu(II) moiety at $g_{\|}$ = 2.27 and $g_{\perp}$ = 2.06 (Figure 8), indicating that there is no delocalization of an electron between the Cu(I) and Cu(II) ions. A conproportionation reaction of a derived mixed-valence complex can be ruled out, because neither product of such a reaction, a dicopper(I) and phenolate (LO)-bridged dicopper(II) complex, would be a simple copper(II) paramagnet. We note that with an unsymmetrical binucleating ligand very similar to LO, L′O, we previously also demonstrated the existence of a mixed-valence dicopper species $[Cu^{II}Cu^{I}(L'O)]^{2+}$ possessing EPR spectroscopic characteristics similar to those observed here.[48]

The kinetics of formation of Fc^{*+} in the second step electron transfer from Fc^* to $[Cu^{II}_2(LO)(OTf)]^{2+}$ (**D1-OTF**) in the presence of HOTF (3.0 mM) in acetone at 213 K (Figure 7) also obeyed pseudo-first-order kinetics (Figure S13 in the

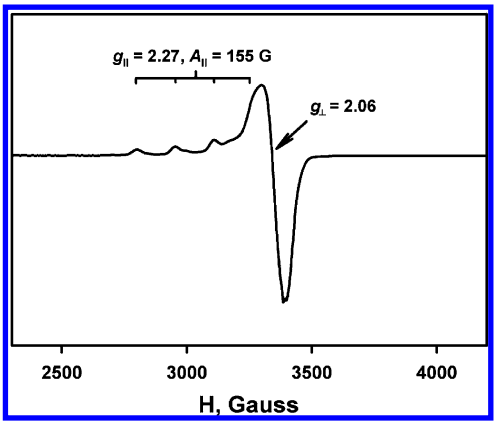

Figure 8. EPR spectrum of $[Cu^{II}Cu^{I}(LO)]^{2+}$ (**D2**) (1.0 mM) recorded in acetone at 5 K. **D2** was generated in the reaction of **D1** (1.0 mM) and Fc^* (1.0 mM) in the presence of HOTF (5.0 mM) in acetone at 298 K. The experimental parameters: microwave frequency = 9.6483 GHz, microwave power = 1.0 mW, and modulation frequency = 100 kHz.

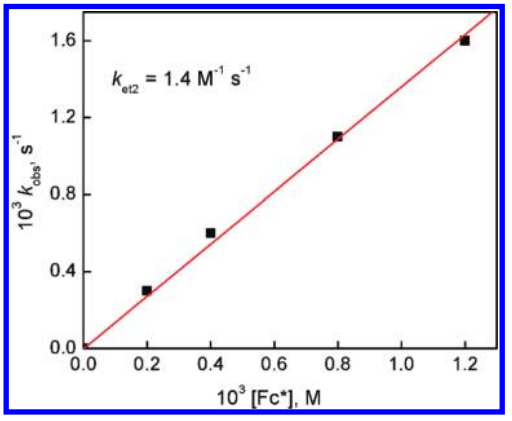

Figure 9. Plot of the pseudo-first-order rate constants (k_{obs}) versus concentrations of Fc^* in the second electron transfer from Fc^* to $[Cu^{II}Cu^{I}(LO)]^{2+}$ (**D2**) (0.10 mM) to determine the k_{et2} value in the presence of HOTF (2.0 mM) in acetone at 213 K.

Supporting Information), and the observed pseudo-first-order rate constant (k_{obs}) also increases linearly with increasing concentration of Fc^* (Figure 9). The second-order rate constant for electron transfer from Fc^* to **D1-OTF** was determined from the slope of a linear plot of k_{obs} versus [Fc^*] to be 1.4 M^{-1} s^{-1} at 213 K. At this temperature, the first step electron transfer was too fast to determine the k_{et1} value. When the temperature is raised to 223 K, the k_{et2} value increased to 5.4 M^{-1} s^{-1}. It is important to note that the k_{et2} value determined from the second step electron transfer from Fc^* to **D1** in the presence of HOTF (2.0 mM) is one-half of the k_1 value (11 M^{-1} s^{-1}) obtained as an intercept in Figure 2b. This clearly indicates that the second step electron transfer from Fc^* to **D1** in the presence of HOTF is the rate-determining step in the catalytic cycle in Scheme 3, because once 1 equiv of Fc^{*+} is formed by electron transfer from Fc^* to **D2**, another equivalent of Fc^{*+} is rapidly formed by the first step electron transfer from Fc^* to **D1-OTF**. In such a case, the rate of formation of Fc^{*+} is derived from Scheme 3 as given by eq 6. By comparing eq 6 with the experimental results (eqs 1 and 2), k_1 in k_{cat} (eq 2) corresponds to $2k_{et2}$, that is, k_{et2} = (1/2)k_1(intercept).

$$d[Fc^{*+}]/dt = 2k_{et2}[\mathbf{D1}][Fc^*] \quad (6)$$

dx.doi.org/10.1021/ja211656g | J. Am. Chem. Soc. 2012, 134, 7025−7035

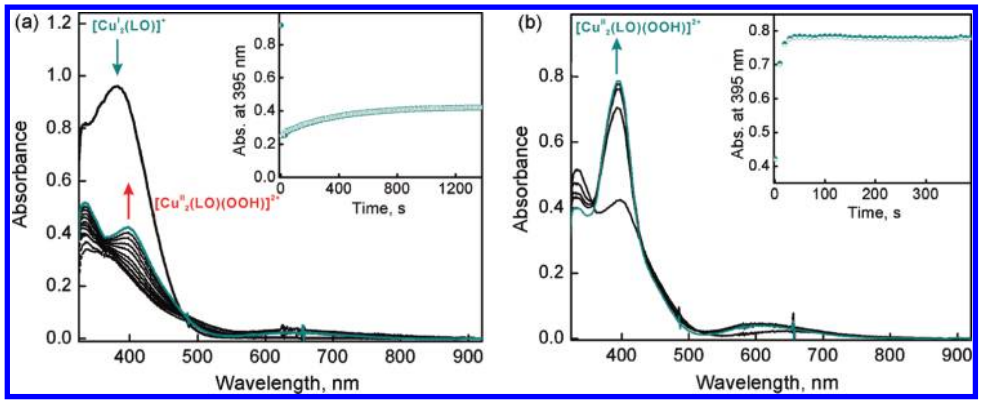

Figure 10. UV−vis spectral changes and time profiles of (a) $[Cu^{I}_2(LO)]^+$ (**D3**) (0.070 mM) after O_2 introduction, demonstrating the generation of $[Cu^{II}_2(LO)(OOH)]^{2+}$ (**D4**) at 395 nm and (b) **D3** (0.070 mM) after O_2 introduction and addition of 1 equiv of HOTF (0.070 mM) in acetone at 193 K.

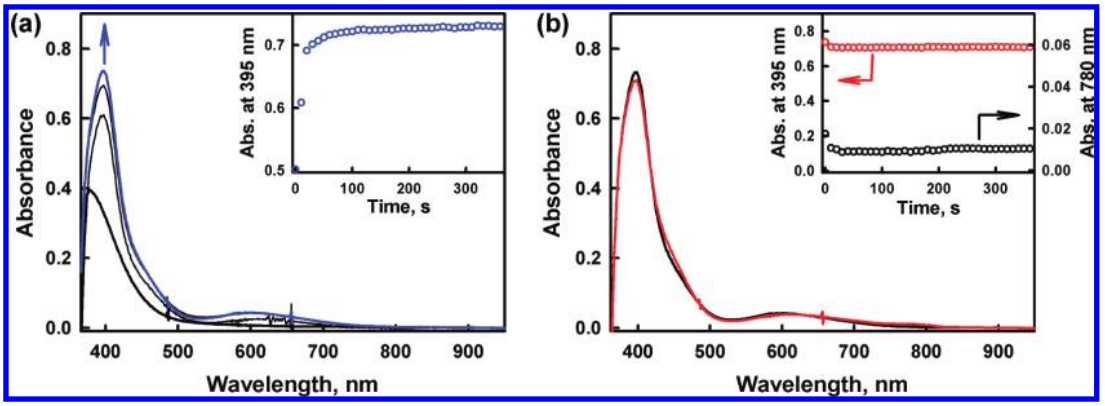

Figure 11. (a) Full formation of the $[Cu^{II}_2(LO)(OOH)]^{2+}$ (**D4**) in an acetone solution containing $[Cu^{I}_2(LO)]^+$ (**D3**) (0.070 mM) and HOTF (0.070 mM) after O_2 introduction at 193 K. Inset shows the absorbance change at 395 nm due to the generated hydroperoxo species. (b) Addition of excess Fc^* (0.28 mM) (red spectrum) to the hydroperoxo species generated (black spectrum) in acetone at 193 K.

The temperature dependence of k_{et2} was examined, and the Eyring plot (Figure S14 in the Supporting Information) afforded the activation enthalpy ($\Delta H^{\ddagger}$ = 11.2 ± 0.2 kcal mol^{-1}) and activation entropy ($\Delta S^{\ddagger}$ = 2 ± 2 cal K^{-1} mol^{-1}). An activation entropy close to zero was previously reported for electron transfer from ferrocene derivatives to Cu(II) complexes.[47]

Cu(II)-Peroxo and -Hydroperoxo Intermediates in the Stoichiometric Two-Electron Reduction of O_2 by Fc^* in the Presence of HOTF. The Cu(II)−oxygen intermediates likely involved in the catalytic two-electron reduction of O_2 by Fc^* in Scheme 3 were examined by following the reaction of an isolated sample of dicopper(I) complex, $[Cu^{I}_2(LO)]^+$ (**D3**), with O_2 at 193 K. When O_2 was introduced to an acetone solution of **D3**, the peroxo complex $[Cu^{II}_2(LO)(OO)]^+$ (**D**), which should form very rapidly (see Introduction), is however slowly converted to the hydroperoxo complex, $[Cu^{II}_2(LO)(OOH)]^{2+}$ (**D4**) as indicated by an increase in the absorption band at 395 nm. This can be explained by the occurrence of the reaction of $[Cu^{II}_2(LO)(OO)]^+$ (**D**) with residual water in acetone (Figure 10a). Instead, when 1 equiv of HOTF is added to the solution containing **D**, the hydroperoxo complex **D4** forms very rapidly (Figure 10b), as expected.[29]

When 1 equiv of HOTF was added before the reaction of $[Cu^{I}_2(LO)]^+$ (**D3**) with O_2, an immediate transformation occurs to give only hydroperoxo complex $[Cu^{II}_2(LO)(OOH)]^{2+}$ (**D4**) (Figure 11a). This indicates that the protonation of the peroxo complex with HOTF is much faster than the formation of the peroxo complex itself. In contrast with the case of μ-η^2:η^2-peroxo dicopper(II) and bis-μ-oxo dicopper(III) complexes, which were readily reduced by Fc^*,[29] no electron transfer from Fc^* to the hydroperoxo complex $[Cu^{II}_2(LO)(OOH)]^{2+}$ (**D4**) occurred as shown in Figure 11b, where the absorption spectrum due to **D4** was not changed by the addition of Fc^*. This is the reason why the selective two-electron reduction of O_2 by Fc^* occurs; that is, the hydroperoxo-dicopper(II) complex **D4** is not susceptible to reduction, and thus with catalyst and HOTF, H_2O_2 is produced.

When HOTF was further added to an acetone solution of $[Cu^{II}_2(LO)(OOH)]^{2+}$ (**D4**), the absorption band due to **D4** disappeared as the concentration of HOTF increased (Figure 12a), indicating that this reaction directly produces $[Cu^{II}_2(LO)(OTF)]^{2+}$ (**D1-OTF**) and hydrogen peroxide. The amount of 10 equiv of HOTF is enough for a quantitative reaction to take place (Figure 12b).

The Reactivity of Mixed-Valence $[Cu^{II}Cu^{I}(LO)]^{2+}$ (D2) with O_2 in the Presence of HOTF. The electron-transfer reduction of $[Cu^{II}_2(LO)(OTF)]^{2+}$ (**D1-OTF**) with Fc^* under single turnover conditions without O_2 clearly shows that the two-electron reduction takes place in two successive steps in which the second step is slower, and this is the rate-determining step in the catalytic cycle in Scheme 3 as described above (see also Figures 5 and 7). Under the catalytic conditions, however, the observed catalytic rate constant (k_{cat}) in the presence of O_2 is larger than twice the rate constant of the second step electron transfer, $k_{cat} > 2k_{et2}$. This suggests that the initial electron-transfer reduction of

dx.doi.org/10.1021/ja211656g | J. Am. Chem. Soc. 2012, 134, 7025−7035

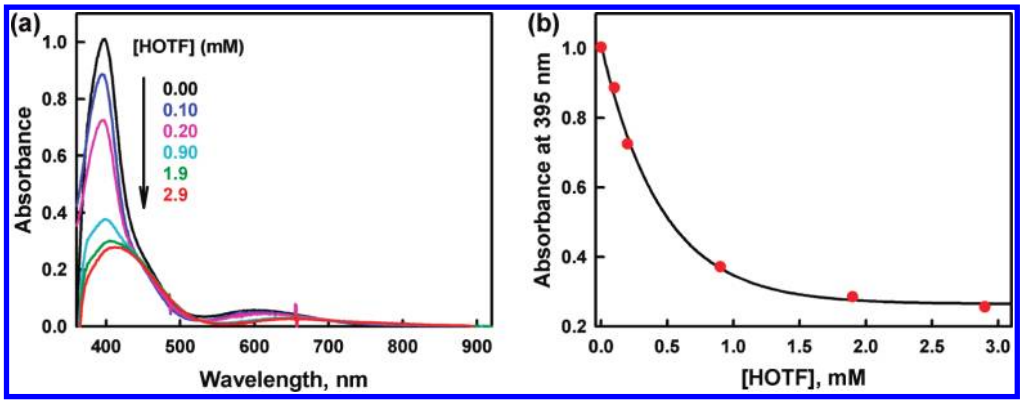

Figure 12. (a) UV−visible spectral changes of $[Cu^{II}_2(LO)(OOH)]^{2+}$ (**D4**) (0.10 mM) in the presence of HOTF (0.10−3.0 mM) in acetone at 193 K. (b) Absorbance changes at 395 nm as a function of HOTF concentration.

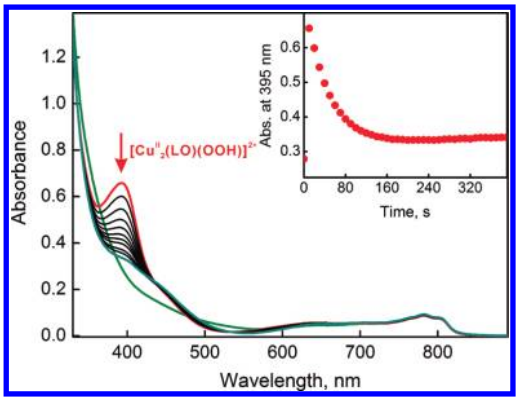

Figure 13. (a) UV−visible spectral changes resulted from introduction of O_2 at 193 K into an acetone solution of $[Cu^{II}Cu^{I}(LO)]^{2+}$ (**D2**) (green spectrum) produced from room-temperature mixing of $[Cu^{II}_2(LO)(OH)]$ (**D1**) (0.10 mM) and Fc^* (0.10 mM) in the presence of HOTF (1.0 mM). The inset shows the time profile of the absorbance at 395 nm due to the $[Cu^{II}_2(LO)(OOH)]^{2+}$ (**D4**) generated (red spectrum).

D1-OTF may be followed by the reaction with O_2 in addition to a second-step electron transfer. This possibility was tested by directly examining the reactivity of the mixed-valence $[Cu^{II}Cu^{I}(LO)]^{2+}$ (**D2**) species with O_2 and in the presence of HOTF.

When O_2 is introduced to an acetone solution of $[Cu^{II}Cu^{I}(LO)]^{2+}$ (**D2**) at 193 K, the hydroperoxo complex $[Cu^{II}_2(LO)(OOH)]^{2+}$ (**D4**) is immediately formed (Figure 13) and is then protonated in the presence of excess acid to give off hydrogen peroxide (see the inset of Figure 13). The amount of **D4** produced is about one-half of the amount of **D2** judging from a comparison of the results in Figure 13 with those in Figure 11. This indicates that the reaction of **D2** with O_2 affords an O_2-adduct of **D2**, a putative superoxo-dicopper(II) species $[Cu^{II}_2(LO)(O_2^{\bullet-})]^{2+}$ ($\mathbf{Cu^{II}_2(O_2^{\bullet-})}$), which is reduced by a second molecule of $[Cu^{II}Cu^{I}(LO)]^{2+}$ (**D2**) and then protonated to give ∼0.5 equiv of **D4**. Under catalytic conditions, however, $[Cu^{II}_2(LO)(O_2^{\bullet-})]^{2+}$ may be reduced by Fc^* that is present to produce 1 equiv of **D4**. Thus, the full catalytic cycle may not actually proceed via dicopper(I) complex $[Cu^{I}_2(LO)]^{+}$ (**D3**) or peroxodicopper(II) complex $[Cu^{II}_2(LO)(OO)]^{+}$ (**D**), but is "short-circuited" as shown in Scheme 4 (and this is also included in Scheme 3).

Protonation versus Electron-Transfer Reduction of $[Cu^{II}_2(LO)(OOH)]^{2+}$ (D4). Concerning the fact that **D4** undergoes protonation releasing hydrogen peroxide, rather than reductive cleavage by Fc^*, as do complexes with a dioxygen-derived "trans"-μ-1,2-peroxo dicopper(II) (**A**), μ-η^2:η^2-peroxo dicopper(II) (**B**), or bis-μ-oxo dicopper(III) (**C**) structure (see Introduction), one can consider a number of points. For one thing, see the DFT-optimized structure of **D4** shown in Figure 14 together with the LUMO orbital (for the calculation, see the Experimental Section). The optimized structure does possess a μ-1,1-OOH ligand as previously proposed on the basis of physical-spectroscopic methods, and the two calculated $Cu-O_{hydroperoxo}$ distances in $[Cu^{II}_2(LO)(OOH)]^{2+}$

Scheme 4

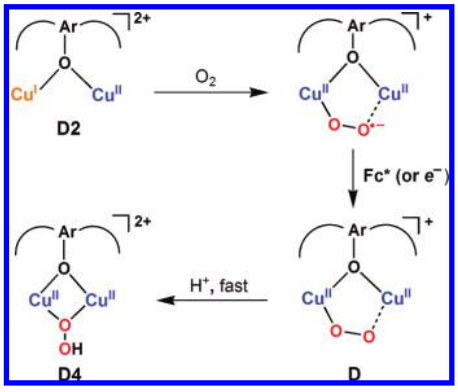

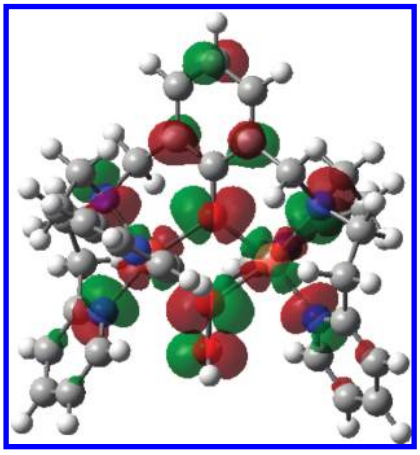

Figure 14. Optimized structure with LUMO of $[Cu^{II}_2(LO)(OOH)]^{2+}$ (**D4**) calculated by DFT B3LYP/lanl2dz basis set.

dx.doi.org/10.1021/ja211656g | J. Am. Chem. Soc. 2012, 134, 7025−7035

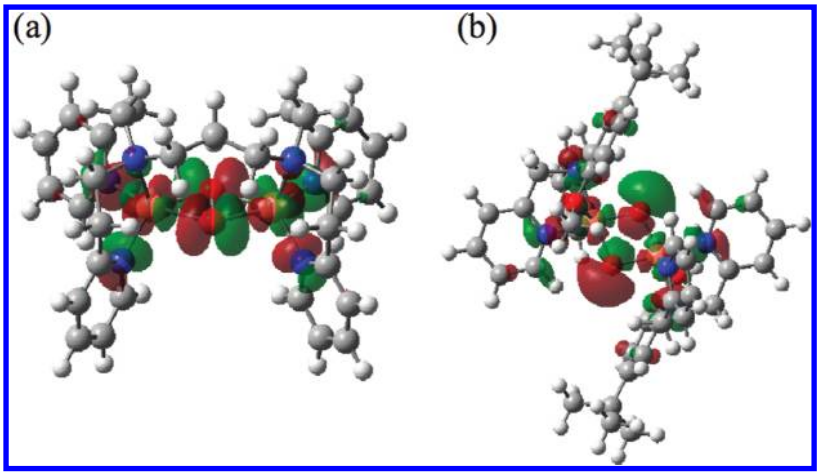

Figure 15. Optimized structures with LUMO of (a) $[Cu^{II}_2(N3)(O_2)]^{2+}$ calculated and (b) $[(BzPY1)Cu^{III}(BzPY1)(O)_2Cu^{III}(BzPY1)]^{2+}$ by DFT B3LYP/Lanl2dz.

(**D4**) are nearly the same (2.044 and 2.046 Å). Because the LUMO orbital is delocalized to not only the metal but also to the ligands, the one-electron reduction of **D4** may not (and does not) lead to O−O bond cleavage for the further reduction to water. Instead, $[Cu^{II}_2(LO)(OOH)]^{2+}$ (**D4**) releases H_2O_2 upon protonation.

Another point is that it has been shown that in copper complexes the O−O bond becomes stronger upon protonation (−OOH) or alkylation (−OOR).[49] Thus, a relatively stronger O−O bond would in the presence of protons undergo copper−O cleavage giving H_2O_2 rather than O−O cleavage eventually leading to water (and the $4e^-/4H^+$ reduction of O_2). The bonding within a μ-η^2:η^2-peroxo dicopper(II) Cu_2O_2 core is well-known to produce very weak O−O bonds, possessing ν(O−O) = 710−760 cm^{-1} (see Scheme 2). Thus, such complexes would be more susceptible to O−O reductive cleavage by Fc^* and protons, just as we have recently reported for the case of $[Cu^{II}_2(N3)(\mu\text{-}\eta^2\text{:}\eta^2\text{-}O_2^{2-})]^{2+}$ (see Introduction).[17b,50] This is further supported by calculations on the LUMO of $[Cu^{II}_2(N3)(\mu\text{-}\eta^2\text{:}\eta^2\text{-}O_2^{2-})]^{2+}$ (Figure 15a), which show it to be mainly localized at the antibonding O−O bond orbitals. Also, $[\{(BzPY1)Cu^{III}\}_2(\mu\text{-}O^{2-})_2]^{2+}$, formed from reduction of $[Cu^{II}(BzPY1)(EtOH)](ClO_4)_2$ (**C1**) and which promotes bis-μ-oxo-dicopper(III) formation, as in this case, would likely promote $4e^-/4H^+$ reduction of O_2. Note that for $[\{(BzPY1)Cu^{III}\}_2(\mu\text{-}O^{2-})_2]^{2+}$, the LUMO is mainly localized at the cleaved oxygen atom orbitals (Figure 15b).

What is perhaps a puzzle at this point is that the (TMPA)−copper system, which provides for chemistry leading to $[\{(TMPA)Cu^{II}\}_2(\mu\text{-}1,2\text{-}O_2^{2-})]^{2+}$ (**A1**), also gives rise to O−O reductive cleavage chemistry (vide supra).[17a] Yet, the O−O bond in this complex is strong, ν(O−O) ≈ 830 cm^{-1}.[51] One may conjecture that the peroxo group in **A1** is well protected relative to the −OOH group in $[Cu^{II}_2(LO)(OOH)]^{2+}$ (**D4**), and that protonation of the latter is extremely fast, while for **A1**, outer-sphere proton-coupled electron-transfer reduction by Fc^* easily proceeds. Certainly other factors may come into play, and a more rigorous experimental and theoretical understanding concerning preference for protonation or reduction surely will come about as more examples of both $4e^-/4H^+$ O_2-reduction to water and $2e^-/2H^+$ reduction of O_2 to hydrogen peroxide are found and investigated in detail.

SUMMARY AND CONCLUSION

A binuclear copper(II) complex ($[Cu^{II}_2(LO)(OH)]^{2+}$) acts as an efficient catalyst for the selective two-electron reduction of O_2 by Fc^* with HOTF in acetone as shown in Scheme 3. The protonation of $[Cu^{II}_2(LO)(OH)]^{2+}$ with HOTF results in formation of $[Cu^{II}_2(LO)(OTF)]^{2+}$, which can be reduced by Fc^* via two-step electron-transfer reactions to produce $[Cu^{I}_2(LO)]^{+}$ via the mixed valence complex $([Cu^{II}Cu^{I}(LO)]^{2+}$. Binuclear Cu(I) complex $[Cu^{I}_2(LO)]^{+}$ reacts with O_2 rapidly in the presence of HOTF to produce the hydroperoxo complex ($[Cu^{II}_2(LO)(OOH)]^{+}$) via protonation of an intermediate peroxo complex ($[Cu^{II}_2(LO)(OO)]$). Further protonation of $[Cu^{II}_2(LO)(OOH)]^{+}$ with HOTF produces H_2O_2, accompanied by regeneration of $[Cu^{II}_2(LO)(OTF)]^{2+}$. The rate-determining step in the predominant catalytic cycle given in Scheme 3 is the second step electron transfer, thus Fc^* reduction of a mixed-valent complex $[Cu^{II}Cu^{I}(LO)]^{2+}$ where this is coupled with O_2-binding to produce peroxo complex $[Cu^{II}_2(LO)(OO)]^{+}$. However, another reaction pathway consists of direct O_2-reaction with $[Cu^{II}Cu^{I}(LO)]^{2+}$, followed by electron-transfer reduction of an O_2-adduct that must be formed, to give peroxo complex $[Cu^{II}_2(LO)(OO)]^{+}$ (Scheme 4).

This is the first selective two-electron reduction of O_2 by a one-electron reductant with a copper complex acting as a catalyst. Future modifications of the supporting ligand may improve the catalytic activity for the selective two-electron reduction of O_2 to H_2O_2, the latter being a promising candidate as a renewable and clean energy source.[30−32]

ASSOCIATED CONTENT

Supporting Information

Figures S1−S14. This material is available free of charge via the Internet at http://pubs.acs.org.

AUTHOR INFORMATION

Corresponding Author

fukuzumi@chem.eng.osaka-u.ac.jp; karlin@jhu.edu; wwnam@ewha.ac.kr

Notes

The authors declare no competing financial interest.

■ ACKNOWLEDGMENTS

The research at OU was supported by a Grant-in-Aid (No. 20108010 and 23750014) and the Global COE program, "the Global Education and Research Center for Bio-Environmental Chemistry" from the Ministry of Education, Culture, Sports, Science and Technology, Japan (to S.F.), and the research at EWU was supported by NRF/MEST of Korea through CRI (to W.N.), GRL (2010-00353) (to W.N.), 2011 KRICT OASIS project (to W.N.), and WCU (R31-2008-000-10010-0) (to W.N., S.F., and K.D.K.). K.D.K. also acknowledges support from the U.S. National Institutes of Health grant GM28962.

■ REFERENCES

(1) (a) Solomon, E. I.; Ginsbach, J. W.; Heppner, D. E.; Kieber-Emmons, M. T.; Kjaergaard, C. H.; Smeets, P. J.; Tian, L.; Woertink, J. S. *Faraday Discuss.* **2011**, *148*, 11−39. (b) Solomon, E. I.; Sundaram, U. M.; Machonkin, T. E. *Chem. Rev.* **1996**, *96*, 2563−2605. (c) Solomon, E. I.; Chen, P.; Metz, M.; Lee, S.-K.; Palmer, A. E. *Angew. Chem., Int. Ed.* **2001**, *40*, 4570−4590. (d) *Bioinorganic Chemistry of Copper*; Karlin, K. D., Tyeklár, Z., Eds.; Chapman & Hall: New York, 1993. (e) Karlin, K. D.; Zuberbühler, A. D. Formation, Structure and Reactivity of Copper Dioxygen Complexes. In *Bioinorganic Catalysis*, 2nd ed.; Reedijk, J., Bouwman, E., Eds.; Marcel Dekker, Inc.: New York, 1999; pp 469−534. (f) Quant Hatcher, L.; Karlin, K. D. *J. Biol. Inorg. Chem.* **2004**, *9*, 669−683. (g) Lee, Y.; Karlin, K. D. Highlights of Copper Protein Active-Site Structure/Reactivity and Synthetic Model Studies. In *Concepts and Models in Bioinorganic Chemistry*; Metzler-Nolte, N., Kraatz, H.-B., Eds.; Wiley-VCH: New York, 2006; pp 363−395.

(2) (a) Holm, R. H.; Kennepohl, P.; Solomon, E. I. *Chem. Rev.* **1996**, *96*, 2239−2314. (b) Karlin, K. D. *Science* **1993**, *261*, 701−708. (c) Metzler-Nolte, N.; Kraatz, H.-B. *Concepts and Models in Bioinorganic Chemistry*; Wiley-VCH: New York, 2006.

(3) (a) Mirica, L. M.; Ottenwaelder, X.; Stack, T. D. P. *Chem. Rev.* **2004**, *104*, 1013−1045. (b) Lewis, E. A.; Tolman, W. B. *Chem. Rev.* **2004**, *104*, 1047−1076. (c) Itoh, S.; Fukuzumi, S. *Acc. Chem. Res.* **2007**, *40*, 592−600. (d) Itoh, S. *Curr. Opin. Chem. Biol.* **2006**, *10*, 115−122.

(4) (a) Klinman, J. P. *Chem. Rev.* **1996**, *96*, 2541−2561. (b) Klinman, J. P. *J. Biol. Chem.* **2006**, *281*, 3013−3016. (c) Prigge, S. T.; Eipper, B.; Mains, R.; Amzel, L. M. *Science* **2004**, *304*, 864−867. (d) Chen, P.; Solomon, E. I. *Proc. Natl. Acad. Sci. U.S.A.* **2004**, *101*, 13105−13110. (e) Balasubramanian, R.; Smith, S. M.; Rawat, S.; Yatsunyk, L. A.; Stemmler, T. L.; Rosenzweig, A. C. *Nature* **2010**, *465*, 115−119. (f) Chan, S. I.; Yu, S. S.-F. *Acc. Chem. Res.* **2008**, *41*, 969−979.

(5) Humphreys, K. J.; Mirica, L. M.; Wang, Y.; Klinman, J. P. *J. Am. Chem. Soc.* **2009**, *131*, 4657−4663.

(6) Mukherjee, A.; Smirnov, V. V.; Lanci, M. P.; Brown, D. E.; Shepard, E. M.; Dooley, D. M.; Roth, J. P. *J. Am. Chem. Soc.* **2008**, *130*, 9459−9473.

(7) McGuirl, M. A.; Dooley, D. M. Copper Proteins with Type 2 Sites. In *Encyclopedia of Inorganic Chemistry*, 2nd ed.; King, R. B., Ed.; John Wiley & Sons Ltd.: Chichester, 2005; Vol. *II*, pp 1201−1225.

(8) (a) Solomon, E. I.; Augustine, A. J.; Yoon, J. *Dalton Trans.* **2008**, 3921−3932. (b) Messerschmidt, A. *Adv. Inorg. Chem.* **1993**, *40*, 121−185. (c) Rodgers, C. J.; Blanford, C. F.; Giddens, S. R.; Skamnioti, P.; Armstrong, F. A.; Gurr, S. J. *Trends Biotechnol.* **2010**, *28*, 63−72. (d) Kosman, D. *J. Biol. Inorg. Chem.* **2010**, *15*, 15−28. (e) Djoko, K. Y.; Chong, L. X.; Wedd, A. G.; Xiao, Z. *J. Am. Chem. Soc.* **2010**, *132*, 2005−2015.

(9) (a) Ferguson-Miller, S.; Babcock, G. T. *Chem. Rev.* **1996**, *96*, 2889−2907. (b) Yoshikawa, S.; Shinzawa-Itoh, K.; Nakashima, R.; Yaono, R.; Yamashita, E.; Inoue, N.; Yao, M.; Jei-Fei, M.; Libeu, C. P.; Mizushima, T.; Yamaguchi, H.; Tomizaki, T.; Tsukihara, T. *Science* **1998**, *280*, 1723−1729. (c) Michel, H.; Behr, J.; Harrenga, A.; Kannt, A. *Annu. Rev. Biophys. Biomol. Struct.* **1998**, *27*, 329−356. (d) Pereira, M. M.; Sousa, F. L.; Verìssimo, A. F.; Teixeira, M. *Biochim. Biophys. Acta* **2008**, *1777*, 929−934. (e) Yoshikawa, S.; Muramoto, K.; Shinzawa-Itoh, K. *Biochim. Biophys. Acta* **2011**, *1807*, 1279−1286.

(10) (a) Collman, J. P.; Devaraj, N. K.; Decreau, R. A.; Yang, Y.; Yan, Y.-L.; Ebina, W.; Eberspacher, T. A.; Chidsey, C. E. D. *Science* **2007**, *315*, 1565−1568. (b) Collman, J. P.; Decréau, R. A.; Lin, H.; Hosseini, A.; Yang, Y.; Dey, A.; Eberspacher, T. A. *Proc. Natl. Acad. Sci. U.S.A.* **2009**, *106*, 7320−7323. (c) Collman, J. P.; Ghosh, S.; Dey, A.; Decréau, R. A.; Yang, Y. *J. Am. Chem. Soc.* **2009**, *131*, 5034−5035.

(11) Kadish, K. M.; Frémond, L.; Shen, J.; Chen, P.; Ohkubo, K.; Fukuzumi, S.; El Ojaimi, M.; Gros, C. P.; Barbe, J.-M.; Guilard, R. *Inorg. Chem.* **2009**, *48*, 2571−2582.

(12) (a) Hatay, I.; Su, B.; Li, F.; Méndez, M. A.; Khoury, T.; Gros, C. P.; Barbe, J.-M.; Ersoz, M.; Samec, Z.; Girault, H. H. *J. Am. Chem. Soc.* **2009**, *131*, 13453−13459. (b) Partovi-Nia, R.; Su, B.; Li, F.; Gros, C. P.; Barbe, J.-M.; Samec, Z.; Girault, H. H. *Chem.-Eur. J.* **2009**, *15*, 2335−2340. (c) Hatay, I.; Su, B.; Méndez, M. A.; Corminboeuf, C.; Khoury, T.; Gros, C. P.; Bourdillon, M.; Meyer, M.; Barbe, J.-M.; Ersoz, M.; Zális, S.; Samec, Z.; Girault, H. H. *J. Am. Chem. Soc.* **2010**, *132*, 13733−13741.

(13) (a) Partovi-Nia, R.; Su, B.; Méndez, M. A.; Habermeyer, B.; Gros, C. P.; Barbe, J.-M.; Samec, Z.; Girault, H. H. *ChemPhysChem* **2010**, *11*, 2979−2984. (b) Su, B.; Hatay, I.; Trojánek, A.; Samec, Z.; Khoury, T.; Gros, C. P.; Barbe, J.-M.; Daina, A.; Carrupt, P.-A.; Girault, H. H. *J. Am. Chem. Soc.* **2010**, *132*, 2655−2662.

(14) Zagal, J. H.; Griveau, S.; Silva, J. F.; Nyokong, T.; Bedioui, F. *Coord. Chem. Rev.* **2010**, *254*, 2755−2791.

(15) Halime, Z.; Kotani, H.; Li, Y.; Fukuzumi, S.; Karlin, K. D. *Proc. Natl. Acad. Sci. U.S.A.* **2011**, *108*, 13990−13994.

(16) Cracknell, J. A.; Vincent, K. A.; Armstrong, F. A. *Chem. Rev.* **2008**, *108*, 2439−2461.

(17) (a) Fukuzumi, S.; Kotani, H.; Lucas, H. R.; Doi, K.; Suenobu, T.; Peterson, R. L.; Karlin, K. D. *J. Am. Chem. Soc.* **2010**, *132*, 6874−6875. (b) Tahsini, L.; Kotani, H.; Lee, Y.-M.; Cho, J.; Nam, W.; Karlin, K. D.; Fukuzumi, S. *Chem.-Eur. J.* **2012**, *18*, 1084−1093.

(18) (a) Thorum, M. S.; Yadav, J.; Gewirth, A. A. *Angew. Chem., Int. Ed.* **2009**, *48*, 165−167. (b) Thorseth, M. A.; Letko, C. S.; Rauchfuss, T. B.; Gewirth, A. A. *Inorg. Chem.* **2011**, *50*, 6158−6162. (c) McCrory, C. C. L.; Devadoss, A.; Ottenwaelder, X.; Lowe, R. D.; Stack, T. D. P.; Chidsey, C. E. D. *J. Am. Chem. Soc.* **2011**, *133*, 3696−3699.

(19) (a) Fukuzumi, S.; Mochizuki, S.; Tanaka, T. *Inorg. Chem.* **1989**, *28*, 2459−2465. (b) Fukuzumi, S.; Mochizuki, S.; Tanaka, T. *Inorg. Chem.* **1990**, *29*, 653−659. (c) Fukuzumi, S.; Mochizuki, S.; Tanaka, T. *J. Chem. Soc., Chem. Commun.* **1989**, 391−392.

(20) Fukuzumi, S. *Chem. Lett.* **2008**, *37*, 808−813.

(21) Kadish, K. M.; Shen, J.; Fremond, L.; Chen, P.; El Ojaimi, M.; Chkounda, M.; Gros, C. P.; Barbe, J. M.; Ohkubo, K.; Fukuzumi, S.; Guilard, R. *Inorg. Chem.* **2008**, *47*, 6726−6737.

(22) (a) Fukuzumi, S.; Okamoto, K.; Gros, C. P.; Guilard, R. *J. Am. Chem. Soc.* **2004**, *126*, 10441−10449. (b) Fukuzumi, S.; Okamoto, K.; Tokuda, Y.; Gros, C. P.; Guilard, R. *J. Am. Chem. Soc.* **2004**, *126*, 17059−17066.

(23) (a) Rosenthal, J.; Nocera, D. G. *Prog. Inorg. Chem.* **2007**, *55*, 483−544. (b) Rosenthal, J.; Nocera, D. G. *Acc. Chem. Res.* **2007**, *40*, 543−553.

(24) Tyeklár, Z.; Karlin, K. D. *Acc. Chem. Res.* **1989**, *22*, 241−248.

(25) (a) Thyagarajan, S.; Murthy, N. N.; Narducci Sarjeant, A. A.; Karlin, K. D.; Rokita, S. E. *J. Am. Chem. Soc.* **2006**, *128*, 7003−7008. (b) Karlin, K. D.; Tyeklár, Z.; Farooq, A.; Haka, M. S.; Ghosh, P.; Cruse, R. W.; Gultneh, Y.; Hayes, J. C.; Toscano, P. J.; Zubieta, J. *Inorg. Chem.* **1992**, *31*, 1436−1451.

(26) Lucas, H. R.; Li, L.; Sarjeant, A. A. N.; Vance, M. A.; Solomon, E. I.; Karlin, K. D. *J. Am. Chem. Soc.* **2009**, *131*, 3230−3245.

(27) Karlin, K. D.; Cruse, R. W.; Gultneh, Y.; Hayes, J. C.; Zubieta, J. *J. Am. Chem. Soc.* **1984**, *106*, 3372−3374.

(28) (a) Karlin, K. D.; Cruse, R. W.; Gultneh, Y.; Farooq, A.; Hayes, J. C.; Zubieta, J. *J. Am. Chem. Soc.* **1987**, *109*, 2668−2679. (b) Pate, J. E.; Cruse, R. W.; Karlin, K. D.; Solomon, E. I. *J. Am. Chem. Soc.* **1987**, *109*, 2624−2630.

(29) Karlin, K. D.; Ghosh, P.; Cruse, R. W.; Farooq, A.; Gultneh, Y.; Jacobson, R. R.; Blackburn, N. J.; Strange, R. W.; Zubieta, J. *J. Am. Chem. Soc.* **1988**, *110*, 6769−6780.
(30) (a) Yamada, Y.; Fukunishi, Y.; Yamazaki, S.-i.; Fukuzumi, S. *Chem. Commun.* **2010**, *46*, 7334−7336. (b) Jing, X.; Cao, D. X.; Liu, Y.; Wang, G. L.; Yin, J. L.; Wen, Q.; Gao, Y. Y. *J. Electroanal. Chem.* **2011**, *658*, 46−51.
(31) For metal−hydrogen peroxide semifuel cells, see ref 32.
(32) (a) Lei, T.; Tian, Y. M.; Wang, G. L.; Yin, J. L.; Gao, Y. Y.; Wen, Q.; Cao, D. X. *Fuel Cells* **2011**, *11*, 431−435. (b) Hasvold, O.; Storkersen, N. J.; Forseth, S.; Lian, T. *J. Power Sources* **2006**, *162*, 935−942. (c) Patrissi, C. J.; Bessette, R. R.; Kim, Y. K.; Schumacher, C. R. *J. Electrochem. Soc.* **2008**, *155*, B558−B562.
(33) (a) Disselkamp, R. S. *Energy Fuels* **2008**, *22*, 2771−2774. (b) Disselkamp, R. S. *Int. J. Hydrogen Energy* **2010**, *35*, 1049−1053.
(34) (a) Galbács, Z. M.; Csányi, L. J. *J. Chem. Soc., Dalton Trans.* **1983**, 2353−2357. (b) Latimer, W. M. *The Oxidation States of the Elements and their Potentials in Aqueous Solutions*; Prentice-Hall: New York, 1952; p 39.
(35) (a) Abrantes, S.; Amaral, E.; Costa, A. P.; Shatalov, A. A.; Duarte, A. P. *Ind. Crop. Prod.* **2007**, *25*, 288−293. (b) Zeronian, S. H.; Inglesby, M. K. *Cellulose* **1995**, *2*, 265−272.
(36) Li, L.; Lee, S.; Lee, H. L.; Youn, H. J. *BioResources* **2011**, *6*, 721−736.
(37) Armarego, W. L. F.; Chai, C. L. L. *Purification of Laboratory Chemicals*, 5th ed.; Butterworth-Heinemann: Amsterdam, 2003.
(38) Mann, C. K.; Barnes, K. K. *Electrochemical Reactions in Nonaqueous Systems*; Marcel Dekker: New York, 1990.
(39) The O_2 concentration in an O_2-saturated acetone solution (11 mM) was determined by the spectroscopic titration for the photooxidation of 10-methyl-9,10-dihydroacridine by O_2, see: Fukuzumi, S.; Ishikawa, M.; Tanaka, T. *J. Chem. Soc., Perkin Trans. 2* **1989**, 1037.
(40) Battino, R. *Oxygen and Ozone*; Pergamon Press: New York, 1981; Vol. 7.
(41) (a) Mair, R. D.; Graupner, A. J. *Anal. Chem.* **1964**, *36*, 194. (b) Fukuzumi, S.; Kuroda, S.; Tanaka, T. *J. Am. Chem. Soc.* **1985**, *107*, 3020−3027.
(42) (a) Becke, A. D. *J. Chem. Phys.* **1993**, *98*, 5648−5652. (b) Lee, C. T.; Yang, W. T.; Parr, R. G. *Phys. Rev. B* **1988**, *37*, 785−789. (c) Heher, W. J.; Radom, K.; Schleyer, P. v. R.; Pople, J. A. *Ab Initio Molecular Orbital Theory*; Wiley: New York, 1986.
(43) Dennington, R., II; Keith, R.; Millam, J.; Eppinnett, K.; Hovell, W. L.; Gilliland, R. Semichem, Inc.: Shawnee Mission, KS, 2003.
(44) Although the protonation equilibirum was well analyzed by assuming formation of a 1:1 complex between **D1** and HOTF, whether H_2O is still coordinated or not has yet to be clarified. However, ESI-MS analysis of such solutions that have λ_{max} = 420 nm does show a pominent peak corresponding to the monocation $\{[Cu^{II}_2(LO)(OTF)](OTF)\}^+$.
(45) For E_{ox} values of ferrocene derivatives in acetone, see the following reference.
(46) (a) Lee, Y.-M.; Kotani, H.; Suenobu, T.; Nam, W.; Fukuzumi, S. *J. Am. Chem. Soc.* **2008**, *130*, 434−435. (b) Fukuzumi, S.; Kotani, H.; Prokop, K. A.; Goldberg, D. P. *J. Am. Chem. Soc.* **2011**, *133*, 1859−1869. (c) Fukuzumi, S.; Kotani, H.; Suenobu, T.; Hong, S.; Lee, Y.-M.; Nam, W. *Chem.-Eur. J.* **2010**, *16*, 354−361. (d) Comba, P.; Fukuzumi, S.; Kotani, H.; Wunderlich, S. *Angew. Chem., Int. Ed.* **2010**, *49*, 2622−2625.
(47) The activation entropy for electron transfer becomes negative when the electron transfer occurs via an intermediate, see: Fukuzumi, S.; Endo, Y.; Imahori, H. *J. Am. Chem. Soc.* **2002**, *124*, 10974−10975.
(48) Mahroof-Tahir, M.; Karlin, K. D. *J. Am. Chem. Soc.* **1992**, *114*, 7599−7601.
(49) (a) Root, D. E.; Mahroof-Tahir, M.; Karlin, K. D.; Solomon, E. I. *Inorg. Chem.* **1998**, *37*, 4838−4848. (b) Chen, P.; Fujisawa, K.; Solomon, E. I. *J. Am. Chem. Soc.* **2000**, *122*, 10177−10193.
(50) Pidcock, E.; Obias, H. V.; Abe, M.; Liang, H.-C.; Karlin, K. D.; Solomon, E. I. *J. Am. Chem. Soc.* **1999**, *121*, 1299−1308.
(51) Baldwin, M. J.; Ross, P. K.; Pate, J. E.; Tyeklár, Z.; Karlin, K. D.; Solomon, E. I. *J. Am. Chem. Soc.* **1991**, *113*, 8671−8679.